CrossMark

ORIGINAL PAPER

The impact of latent heating on the location and strength of the tropical easterly jet

Samrat Rao[1,2] · Jayaraman Srinivasan[3]

Abstract The tropical easterly jet (TEJ) is a prominent atmospheric circulation feature observed during the Asian summer monsoon. It is generally assumed that sensible heating over the Tibetan Plateau directly influences the location of the TEJ. However, other studies have suggested the importance of latent heating in determining the jet location. In this paper, the relative importance of latent heating on the maintenance of the TEJ is explored through simulations with a general circulation model. The simulation of the TEJ by the Community Atmosphere Model, version 3.1 is discussed in detail. These simulations showed that the location of the TEJ is well correlated with the location of the precipitation. Significant zonal shifts in the location of the precipitation resulted in similar shifts in the zonal location of the TEJ. These zonal shifts had minimal effect on the large-scale structure of the jet. Further, provided that precipitation patterns were relatively unchanged, orography did not directly impact the location of the TEJ. These changes were robust even with changes in the cumulus parameterization. This suggests the potential important role of latent heating in determining the location and structure of the TEJ. These results were used to explain the significant differences in the zonal location of the TEJ in the years 1988 and 2002. To understand the contribution of the latitudinal location of latent heating on the strength of the TEJ, aqua-planet simulations were carried out. It has been shown that for similar amounts of net latent heating, the jet is stronger when heating is in the higher tropical latitudes. This may partly explain the reason for the jet to be very strong during the JJA monsoon season.

✉ Samrat Rao
samrat.rao@gmail.com; samrat.rao@jncasr.ac.in

[1] Department of Mechanical Engineering, Indian Institute of Science, Bangalore 560012, India

[2] Engineering Mechanics Unit, Jawaharlal Centre for Advanced Scientific Research, Bangalore 560064, India

[3] Divecha Centre for Climate Change, Indian Institute of Science, Bangalore 560012, India

1 Introduction

The tropical easterly jet (TEJ) is one of the most defining aspects of the Indian summer monsoon (ISM), itself a prominent feature of the Asian summer monsoon (ASM). The onset and progress of the ISM is shown in Fig. 1. Additional details are in Joseph (2012). The major geographical entities are shown in Fig. 2a, b. It can be seen that by the end of July the monsoon covers the Indian subcontinent. Hence in Fig. 2a, b the wind vectors at 850 and 150 hPa have been shown. In Fig. 2b the 30 m s^{-1} zonal wind contour is also shown. The pressure level of 150 hPa has been selected since this is where the jet maximum occurs (Abish et al. 2013).

The jet is most prominent during the ISM, occurring within the months of June–September and has a great influence on the rainfall in South Asia and Africa (Hulme and Tosdevin 1989; Webster and Fasullo 2003). The correct simulation of TEJ is important for accurate seasonal predictions and weather forecasting.

The TEJ was first documented by Koteswaram (1958). The development of the TEJ is believed to be influenced by the Tibetan Plateau. Previous studies (e.g. Flohn 1968; Krishnamurti 1971) have highlighted the presence of an upper tropospheric anticyclone above the Tibetan Plateau

in summer. The origin of the Tibetan anticyclone itself has been attributed to the summertime insolation on the Tibetan Plateau. Flohn (1965) first suggested that southern and southeastern Tibet act as elevated heat sources in summer, changing the meridional temperature and pressure gradients. This results in the reversal of high tropospheric flow during early June. Flohn (1968) later showed that a combination of sensible heat source over the Tibetan Plateau as

Fig. 1 Normal monsoon onset dates over the south Asian region. The contours indicate a precipitation rate of 6 mm day^{-1} (figure taken from http://weather.ou.edu/~spark/AMON/v1_n2/Yang/)

well as latent heat release due to monsoonal rains over central and eastern Himalayas generate a warm core anticyclone in the upper troposphere near 30°N. This establishes the south Asian monsoonal circulation over southern Asia. According to Koteswaram (1958), these winds are a part of the Tibetan anticyclone which forms during the summer monsoon over South Asia.

Ye (1981) did laboratory experiments to simulate the heating effect of elevated land. He introduced heating in an ellipsoidal block, resulting in a vertical circulation, an anticyclone in the upper layer, and cyclonic flow in the lower layer. The pattern was found to be qualitatively similar to the summer time atmospheric circulation in South Asia. Duan and Wu (2005) and Wang (2006) considered that the elevated heat source of the Tibetan Plateau was instrumental in providing an anchor to locate the Tibetan high.

Raghavan (1973) opined that the TEJ was the upper tropospheric zonal component of the equatorward outflow from the upper tropospheric Tibetan anticyclone. The importance of Tibetan Plateau was examined. According to him, in the summer season, the thermal condition in the lower troposphere above the Tibetan Plateau was not responsible for the upper tropospheric anticyclone. The
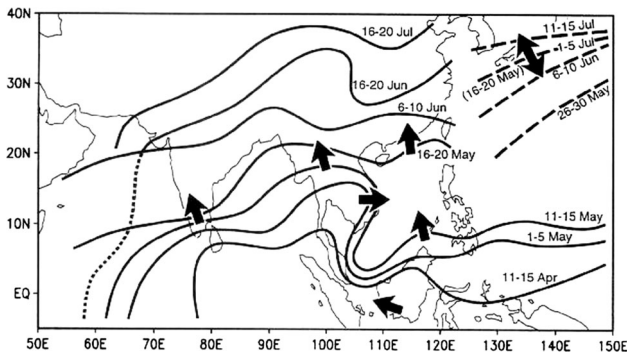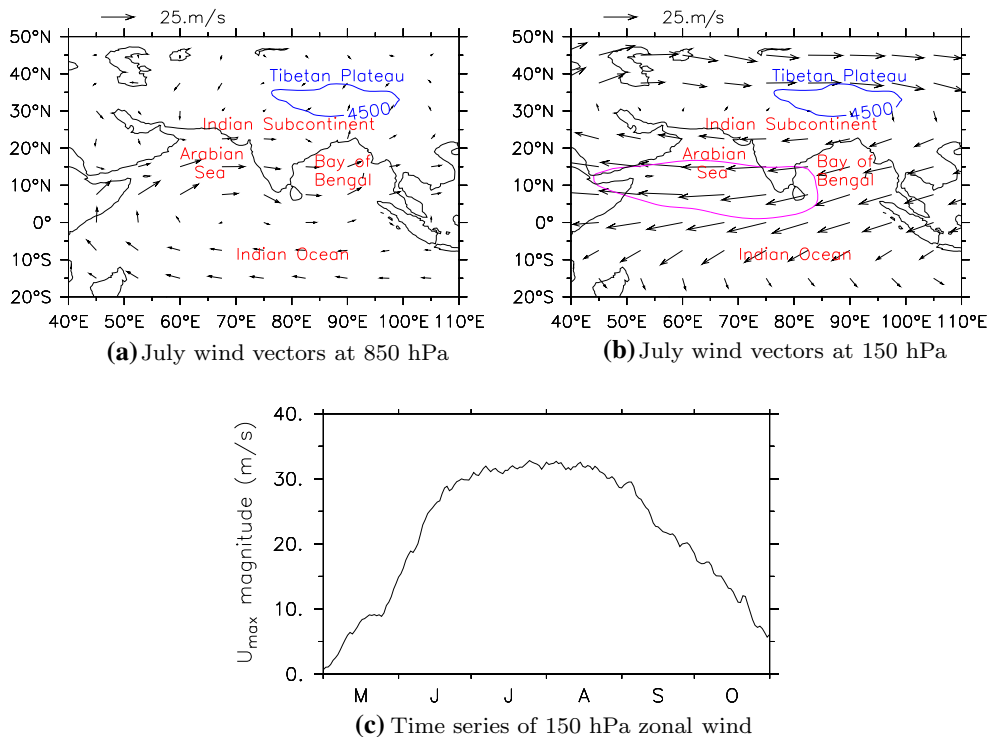

(a) July wind vectors at 850 hPa

(b) July wind vectors at 150 hPa

(c) Time series of 150 hPa zonal wind

Fig. 2 a, **b** Geography and July wind patterns. The *blue contour* indicates the Tibetan Plateau defined by an elevation of 4500 m and above. In **b** the *pink line* denotes the 30 m s^{-1} zonal wind contour. **c** Time series of zonal wind averaged between 50°E and 80°E, 0°N and 15°N at 150 hPa (pressure level where maximum zonal wind is attained, see Table 1) showing TEJ peaking in July–August. All velocity data are from NCEP (averaged for the years 1980–2002). For **c** the averages were calculated from NCEP daily data (color figure online)

Table 1 Magnitude (m s^{-1}) and location of peak zonal wind, and mean (mm day^{-1}) and centroid of precipitation

Case	Zonal wind				Precipitation		
	Peak	Lon (°E)	Lat (°N)	Press	Mean	Lon (°E)	Lat (°N)
Reanalysis and observation							
NCEP	34.48	65.1	10.3	150	5.46	91.6	9.4
ERA40	33.61	68.7	10.4	150	6.06	93.5	9.3
GPCP					4.48	94.4	11.4
CMAP					5.05	94.1	9.6
CAM-3.1 simulations with unmodified cumulus parameterization							
Ctrl	47.19	42.5	8.8	125	6.37	80.4	10.1
noGlOrog	43.45	43.5	7.6	125	6.00	79.8	8.0
CAM-3.1 simulations with modified cumulus parameterization							
Ctrlτ_{d12}	48.79	64.0	7.2	125	6.17	91.3	14.2
noGlOrogτ_{d12}	39.51	64.0	6.0	125	5.63	89.3	11.7
CtrlZM	43.12	49.5	5.6	130	6.23	86.8	12.3
CtrlZMτ_{d3}	46.28	60.5	6.4	125	6.33	90.9	14.1

All values were obtained by computing them for each individual year and then averaging them

Ctrl, Ctrlτ_{d12}, CtrlZM, CtrlZMτ_{d3}: default orography

noGlOrog, noGlOrogτ_{d12}: no orography

anticyclone was absent at 500–250 hPa levels in June and September because at these levels the atmosphere over the plateau was generally cold compared to the adjoining Indian plains. However, at around 100 hPa, the anticyclone was over the Plateau throughout the season from June to September. Thus, Raghavan argued that the presence of the upper tropospheric anticyclone at 150–100 hPa could not be attributed to the sensible and latent heat available over the plateau. He showed that the anticyclone existed at upper levels over south-east Tibet when the plains of India lying to north of the Bay of Bengal were warmer than the Bay of Bengal and its adjoining land areas to the east and west. He further showed that shifting of the monsoon trough during strong and weak monsoon years had a significant influence on the northward extent of the TEJ.

Hoskins and Rodwell (1995) and Liu et al. (2007) have argued that orography plays a secondary role in determining the position of the summertime upper tropospheric anticyclone. Boos and Kuang (2010) showed that removal of the Tibetan Plateau did not effect the large-scale south Asian summer monsoon circulation, provided that the narrow orography of the Himalayas and adjacent mountain ranges were retained. Liu and Yin (2002) suggested that the evolution of the east Asian monsoon is more sensitive to the Tibetan Plateau than the south Asian Monsoon. Chakraborty et al. (2002) used a GCM to demonstrate that the Indian summer monsoon was more influenced by orography to the west of 80°E than by orography to the east of 80°E.

A very simple and elegant mechanism of the direct effects of the TEJ on the Asian monsoonal convection regime was proposed by Webster and Fasullo (2003). In the entrance region, the accelerating limb of the jet induces a secondary circulation via the ageostrophic meridional velocity component, which enhances convection in the Bay of Bengal region. Conversely, similar dynamics in the decelerating limb of the jet acts to suppress convection over North Africa. They hypothesized that this could explain the existence of the most intense rainfall of the Asian monsoon system.

The Tibetan high itself responds to precipitation changes and exhibits intra-seasonal oscillations. Zhang et al. (2002) found that this high pressure system had a bimodal structure. Its two modes, the Tibetan mode and the Iranian mode, both of which were fairly regular in their occurrence, were mostly influenced by heating effects. The former owed its existence to diabatic heating of the Tibetan Plateau, while the latter occurred due to adiabatic heating in the free atmosphere. They reported that the Iranian mode was associated with decreased rainfall pattern in south Japan, Korea and Yangtze-Yellow river valley and the Tibetan Plateau.

The TEJ is not simply a passive atmospheric phenomenon. Its impact on the African monsoon has been documented. Camberlin (1995) showed significant linkages between interannual variations of summer rainfall in Ethiopia-Sudan region and strength and latitudinal extent of upper-tropospheric easterlies. Nicholson et al. (2007) showed that the wave activity along the TEJ influences the African easterly jet (AEJ), a feature that influences the weather patterns over the Atlantic coast of Africa. Lafore and Moncrieff (1989) and Besson and Lemaître (2014)

showed that the interactions between the TEJ and AEJ with convective systems leads to the development and dissipation of such systems over West Africa.

Hulme and Tosdevin (1989) showed that the TEJ responds to El Niño events. Jingxi and Yihui (1989) studied the TEJ at 200 hPa and found that precipitation changes in the west coast of India led to changes in the jet structure. Chen and van Loon (1987) showed that at 200 hPa the jet was weaker during El Niño and Indian drought events. The TEJ was weaker in the drought years of 1979, 1983, and 1987 and stronger in the excess monsoon years of 1985 and 1988.

Based on these results, it is hypothesized that it is monsoonal diabatic heating that exercises a major control on the location and strength of the TEJ. An Atmospheric General Circulation Model (AGCM) is used to study the importance of monsoonal latent heat sources in setting up the thermal gradients that form and maintain the strength and location of the TEJ. In the next section, the model details and numerical simulations are explained. In Sect. 3, the characteristics of the TEJ are presented using reanalysis data. The simulated TEJ using the Community Atmosphere Model, version 3.1 (CAM-3.1) is presented in Sect. 4. The linkage between the spatial distribution of precipitation and the TEJ is explained in Sect. 5. In Sect. 6, the latitudinal impact of latent heating is discussed using aqua-planet simulations.

2 Model details and numerical experiments

2.1 Description of CAM-3.1

The AGCM that was used for the present work is CAM-3.1 (http://www.cesm.ucar.edu/models/atm-cam/). The finite-volume dynamical core using the recommended $2° \times 2.5°$ grid spacing was used for all simulations. The time step was 30 min and 26 vertical levels were used. Deep and shallow convection were parameterized using the Zhang and McFarlane (1995) and Hack (1994) schemes, respectively. Stratiform processes employ the Rasch and Kristjánsson (1998) scheme updated by Zhang et al. (2003). Cloud fraction was computed using a generalization of the scheme introduced by Slingo (1989). The shortwave radiation scheme employed is described in Briegleb (1992). The longwave radiation scheme was from Ramanathan and Downey (1986). Land surface momentum, sensible heat, and latent heat fluxes were calculated from Monin–Obukhov similarity theory applied to the surface. The model was initialized using humidity, winds, temperatures, ice cover and planetary boundary layer height of 1st September 1991. The climatological mean sea-surface temperature (SST) was specified as the boundary condition. Sea surface temperatures were calculated by combining the global Hadley Centre Sea Ice and Sea Surface Temperature (HadISST) dataset (Rayner et al. 2003 for years up to 1981, and Reynolds et al. 2002 for data after 1981).

2.2 Experiment details

The model in its default configuration was run for 5-year period. This simulation is referred to as the control (Ctrl) simulation. Additionally, another simulation (referred to as noGlOrog) was conducted to check the influence of orography on the TEJ. This was also run for 5 years with the same initial and boundary conditions, but with orography all over the globe removed. This latter simulation was used to investigate the direct influence of topography on the TEJ.

Additional simulations were used to test the sensitivity of the TEJ to the convective parameterization. Two types of changes were made to the cumulus parameterization:

1. Changing the convective relaxation time scale for deep convection (τ_d) from the default value of 1–12 h. This parameter had an important influence on the precipitation pattern. Two simulations were conducted with this new relaxation time scale—one with default orography (Ctrlτ_{d12}) and one without orography (noGlOrogτ_{d12}). No other changes were made.

2. Replacing Zhang–MacFarlane scheme of CAM-3.1 with that of CAM-5.0 which is a part of Community Earth System Model, version 1.0.2 (CESM-1.0.2). The incorporation of a more modern and improved cumulus scheme into a relatively older model, CAM-3.1, enabled us to further study the impact of latent heating on the location and strength of the TEJ. The Zhang–MacFarlane scheme of CESM-1.0.2 was different from the scheme of CAM-3.1 in two ways:

   (a) It had a new formulation that used moist entropy conservation and mixing methods of Raymond and Blyth (1986, 1992). This resulted in increased convection sensitivity to tropospheric moisture.

   (b) Sub-grid scale convective momentum transports were added to the deep convection scheme following Richter and Rasch (2008) and the methodology of Gregory et al. (1997).

   This simulation has been named as CtrlZM. In this newer Zhang–MacFarlane scheme, the default value of τ_d was 1 h. An additional simulation with τ_d changed to 3 h was conducted. This simulation is named as CtrlZMτ_{d3}.

The results obtained from the above simulations were based on 5-year mean. For all simulations, other than

removing orography whenever mentioned, the initial conditions were the same as that of Ctrl simulation.

To gain an insight into some of the simulations, the aqua-planet configuration of CAM-3.1 was used. The aqua-planet simulations have all land points replaced by ocean points. These simulations had no seasonal and diurnal cycles. Since the focus was on understanding the role of summer monsoonal heat sources on the location and strength of the TEJ, two simulations with a single heat source were conducted. The off-equatorial monsoonal summer-time heat sources in the Bay of Bengal were imitated by elevating SSTs in circular-shaped regions (radius 10°) centered at (1) 90°E, 10°N and (2) 90°E, 20°N. The center points had a peak SST of 32 °C. These peak SST values were linearly brought down to 20 °C. The SSTs were held constant throughout the period of integration. This makes the configuration similar to the aqua-planet simulations by Chakraborty et al. (2008). The names of these two aqua-planet simulations are AP_90e10n and AP_90e20n, respectively. The initial conditions were from the first year's 1st January Ctrl run results. The default value of $\tau_d = 1$ h was retained. The results of these simulations were based on 6 month averages after discarding the first 6 months data.

3 Characteristics of the tropical easterly jet: reanalysis data

The reanalysis data used for the wind fields were National Centers for Environmental Prediction (NCEP) reanalysis data (Kalnay et al. 1996) and European Centre for Medium-Range Weather Forecasts 40-year Re-analysis (ERA40) data (Uppala et al. 2005). The precipitation data were taken from Global Precipitation Climatology Project (GPCP) (Adler et al. 2003), CPC Merged Analysis of Precipitation (CMAP) (Xie and Arkin 1997) and also from NCEP. Unless otherwise mentioned, the time period examined in this study was 1980–2002. As an exception, precipitation and zonal wind for July 1988 and 2002 were also examined. In the present work, the focus is on the TEJ during the month of July when it first reaches its maximum value, as shown in Fig. 2c. The pressure level of 150 hPa was examined, the level of the zonal wind maximum (Abish et al. 2013).

The magnitude of peak zonal wind and its location are listed in Table 1. Due to the good agreement in the location and strength of the TEJ for NCEP and ERA40, reanalyses of only the former are shown. Although there is a difference of $\sim 3°$ in the zonal location of peak zonal wind (henceforth U_{max}) between the two datasets, the difference is relatively insignificant for the purpose of this study. Figure 3a shows the zonal wind and location of U_{max} for NCEP at 150 hPa. The meridional cross section of the zonal wind at the longitude where the zonal wind is maximum is shown in Fig. 3b. Henceforth, unless otherwise mentioned, all cross sections are at the location of U_{max}. The meridional structure shows the jet peak lying between 0°N and 20°N. There is a vertical equator to pole tilt in the jet, with higher mean height of maximum easterly zonal winds located at higher latitudes. Figure 3c confirms that the peak of the geopotential height (Z) is not located over the Tibetan Plateau, but rather to the west of it. As expected, geostrophic approximation for the zonal wind

Fig. 3 NCEP data. **a** Zonal wind contours at pressure level where U_{max} is attained, *cross-diamond* is location of U_{max}; **b** meridional cross section of zonal wind at U_{max} longitude; **c** negative of meridional gradient of geopotential height (Z) divided by Coriolis parameter ($-\frac{1}{f}\frac{\partial Z}{\partial y}$, s) (*shaded*), and Z contour ($\times 10^3$ m) (*continuous blue line*), *star* is location of peak Z (Z_{max}), Z contour is 14.36 which is 99.5 % of Z_{max}. *Cross-diamond* is the location of U_{max}. All figures for the month of July averaged for the years 1980–2002 (color figure online)

(a) July zonal wind (150 hPa)

(b) July zonal wind (65.1°E)

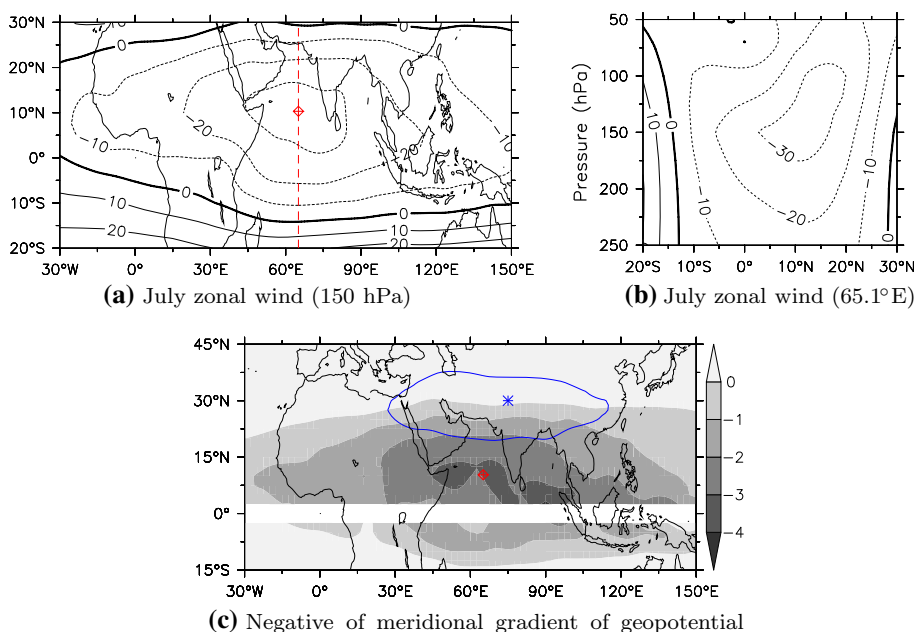**(c)** Negative of meridional gradient of geopotential

Fig. 4 **a** 30 m s^{-1} zonal wind contour in July 1988 and 2002 showing shift in TEJ in response to heating, cross-section is at 150 hPa which is the pressure level where U_{max} is attained, *cross-diamond* shows the location of maximum zonal wind; **b**, **c** meridional cross sections of zonal wind contours in July 1988 and 2002 at the meridional location of U_{max}. All data from NCEP (color figure online)
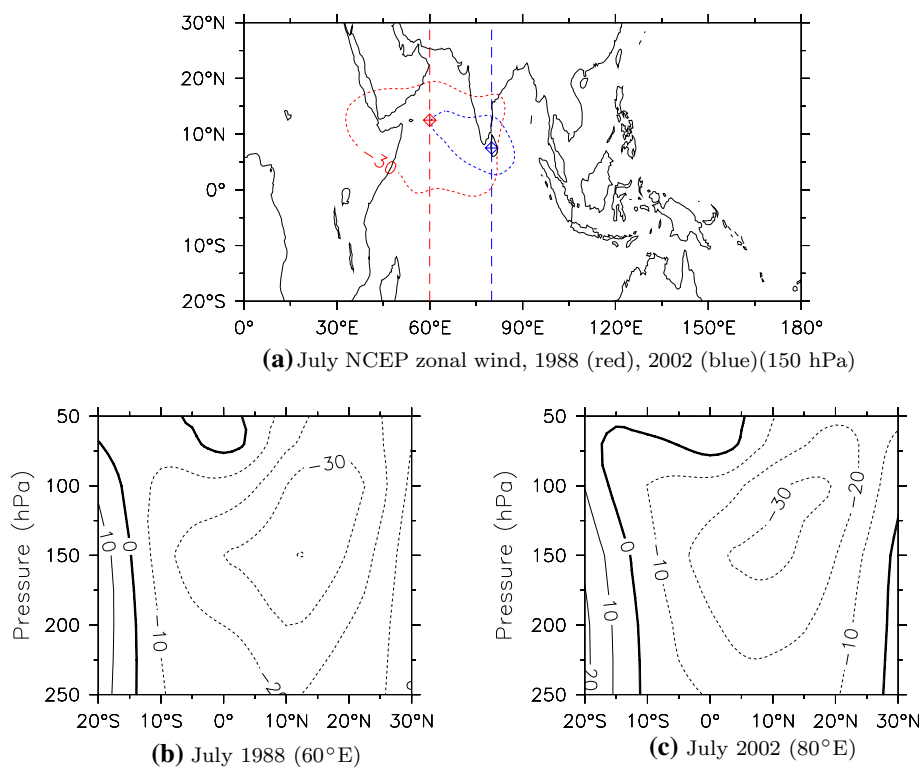

(a) July NCEP zonal wind, 1988 (red), 2002 (blue)(150 hPa)

(b) July 1988 (60°E)

(c) July 2002 (80°E)

Fig. 5 **a**, **c** July zonal wind at pressure level where U_{max} is attained, *cross-diamond* is location of peak zonal wind; **b**, **d** July zonal wind at longitude where U_{max} is attained. Data from simulations have been averaged for the month of July of five consecutive years. Details are in Table 1 (color figure online)

(a) July Ctrl (125 hPa)

(b) July Ctrl (42.5°E)

(c) July noGlOrog (125 hPa)

(d) July noGlOrog (43.5°E)
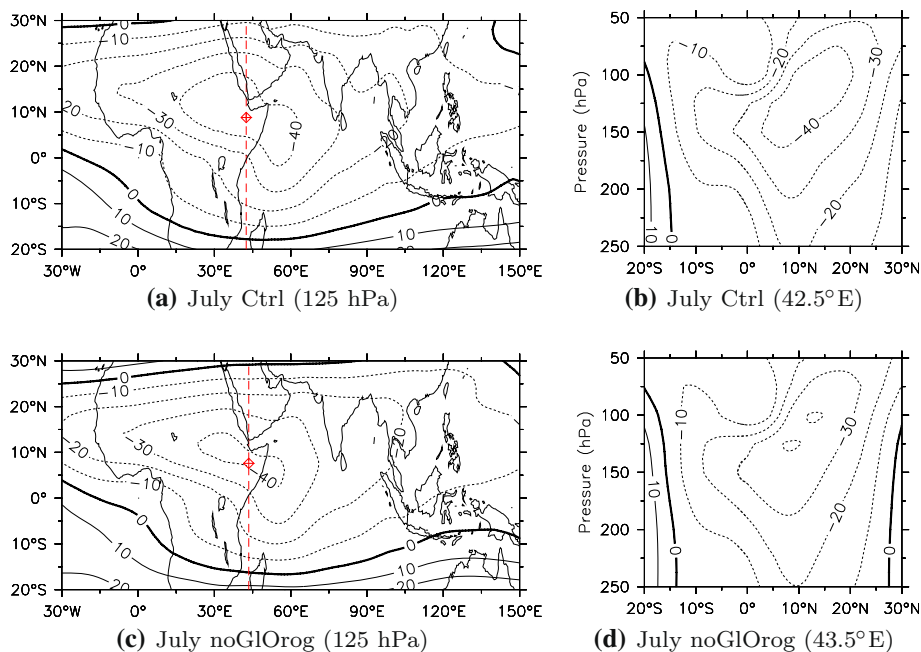
shows that the TEJ reaches its maximum in regions close to geostrophic zonal wind maxima.

The TEJ is not a stationary entity. Variations in its position have been observed. As an example, this can be seen by comparing the jet in July 1988 and 2002. The location of the TEJ for these 2 years is radically different. This is seen in Fig. 4a where the 30 m s^{-1} zonal wind contour and U_{max} locations show significant differences. The location of U_{max} is shifted eastwards by $\sim 20°$ in 2002 relative to 1988. These differences were observed in ERA40 data as well (not shown). The meridional vertical

structure for these 2 years are shown in Fig. 4b, c. Both are similar to Fig. 3b. Although the horizontal pattern of the TEJ shows significant zonal shifts, the vertical structure is similar for the 2 years.

4 The tropical easterly jet in CAM-3.1

4.1 Ctrl simulation

Figure 5 shows a planar and a meridional cross-sectional view of the TEJ for Ctrl simulation. A TEJ can be observed, and is shifted approximately 30° westward compared to reanalysis data. This shift was also documented by Hurrell et al. (2006), where they analyzed the 200 hPa JJA zonal wind fields from CAM-3 simulations. The zonal extent of the simulated TEJ is much larger, while the meridional cross section is very similar to the reanalysis data. The TEJ is stronger in Ctrl by approximately 15 m s^{-1} compared to reanalysis data. Figure 6a shows the geopotential height and its meridional gradient divided by the Coriolis parameter. The peak is shifted westwards in comparison to NCEP (Fig. 3c), and consistent with the westward shift of the TEJ.
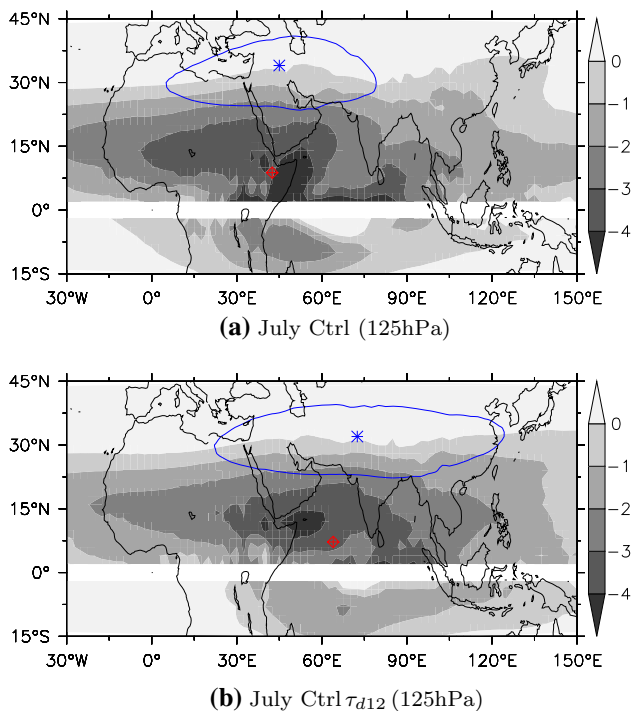

(a) July Ctrl (125hPa)

(b) July Ctrl τ_{d12} (125hPa)

Fig. 6 Negative of meridional gradient of geopotential height (Z) divided by Coriolis parameter ($-\frac{1}{f}\frac{\partial Z}{\partial y}$, s) (*shaded*), and Z contour ($\times 10^3$ m) [*continuous (blue) line*], *star* is location of peak Z (Z_{max}). Z contour for Ctrl and Ctrl$_{d12}$ is 15.62 and 15.57, respectively, which is 99.5 % of individual peak. *Cross-diamond* is the location of U_{max}. Data from simulations have been averaged for the month of July of five consecutive years (color figure online)

4.2 noGlOrog simulation

Figure 5c, d shows the horizontal and meridional profiles of the TEJ for noGlOrog simulation. In the absence of orography, the location of the peak zonal wind is virtually the same for Ctrl and noGlOrog simulations, although the jet is slightly weaker.

4.3 Impact of cumulus parameterization on the simulated TEJ

The large westward shift of the simulated TEJ leaves open the question whether the heating due to the Tibetan Plateau is too far away to influence the jet. A more revealing situation would be to come up with simulations in which the TEJ is located in its climatological position with and without orography. This will be beneficial as the importance of the Tibetan Plateau in anchoring the TEJ can be better understood.

This effect is demonstrated by making a simple change in the Zhang–MacFarlane deep-convective scheme of CAM-3.1. This change affects precipitation by altering the closure criteria used in Zhang–MacFarlane scheme. The closure criteria used in Zhang–MacFarlane scheme is:

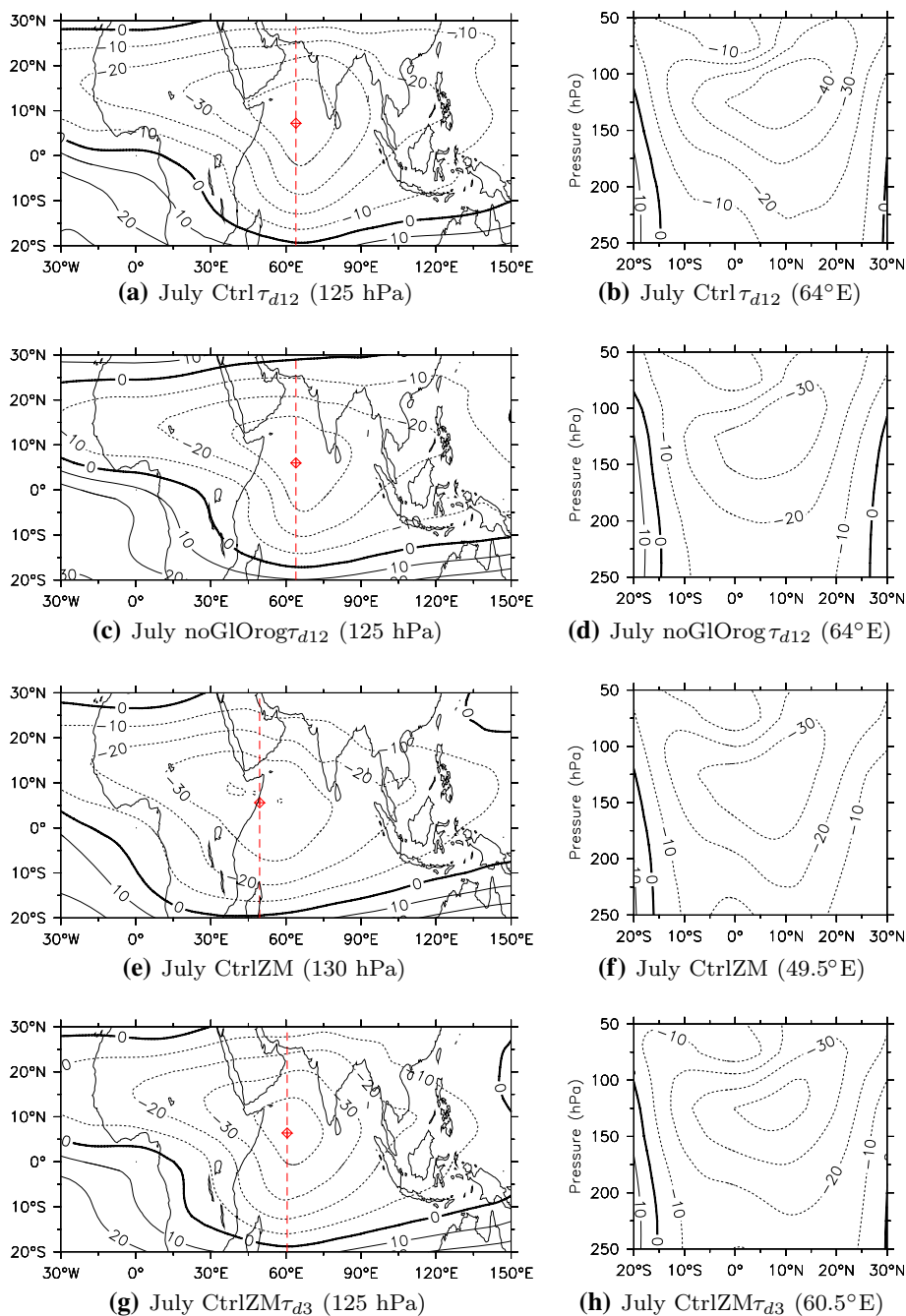$$M_b \propto (\text{CAPE}) \times \tau_d^{-1}$$

where,

M_b	cloud base mass flux
CAPE	convective available potential energy

It can be seen that a specified adjustment time scale, τ_d, determines the cloud base mass flux. As τ_d increases, it will reduce M_b, and hence the rate at which CAPE is consumed decreases. Hence, altering the value of τ_d was considered. Bretherton et al. (2004) had discussed the impact of τ_d in their model simulations. They suggested using a value of 12 h for a horizontal model resolution of 300 km. A more detailed study of the influence of τ_d on the mean tropical climate produced by CAM-3.0 is in Mishra (2008, 2010). More recently, Jain et al. (2011) studied the impact of relaxation parameter on the simulated precipitation of a GCM using the relaxed Arakawa–Schubert convection scheme. They found that a high relaxation time-scale was more appropriate for simulating better precipitation in the Indian region.

4.3.1 Impact of changes in Zhang–MacFarlane scheme of CAM-3.1

The horizontal zonal wind profiles, at U_{max} pressure level, of Ctrlτ_{d12} (default orography) and noGlOrogτ_{d12} (no orography) are shown in Fig. 7a, c. In both simulations, the TEJ is now in the correct location and matches closely with

Fig. 7 a, c, e, g July zonal wind at pressure level where U_{max} is attained, *cross-diamond* is location of peak zonal wind; **b, d, f, h** July zonal wind at longitude where U_{max} is attained. Data from simulations have been averaged for the month of July of five consecutive years. Details are in Table 1 (color figure online)

(a) July Ctrlτ_{d12} (125 hPa)

(b) July Ctrlτ_{d12} (64°E)

(c) July noGlOrogτ_{d12} (125 hPa)

(d) July noGlOrogτ_{d12} (64°E)

(e) July CtrlZM (130 hPa)

(f) July CtrlZM (49.5°E)

(g) July CtrlZMτ_{d3} (125 hPa)

(h) July CtrlZMτ_{d3} (60.5°E)

NCEP (Fig. 3a). The lack of difference in spatial structure of the jet between Ctrlτ_{d12} and noGlOrogτ_{d12} again confirms that if the location of latent heating does not vary, orography has a limited role to play in maintaining the jet location. The magnitude of zonal winds speeds are ~ 10 m s^{-1} less in noGlOrogτ_{d12} simulation. Overall, the jet shows the same characteristics of narrow entry and exit region. The meridional wind profile of Ctrlτ_{d12} and noGlOrogτ_{d12} simulations (Fig. 7b, d) also has the same shape as NCEP and Ctrl. The geopotential height contour and its meridional gradient for Ctrlτ_{d12} is shown in Fig. 6b and is similar

to NCEP. Although it appears that orography has a direct impact in reducing the strength of the TEJ, it is shown in Sect. 6 that this is due to change in the location of precipitation in region beyond 20°N.

4.3.2 Impact of Zhang–MacFarlane scheme of CESM-1.0.2

From Table 1, it can be seen that in the CtrlZM simulation, the zonal wind is displaced $\sim 7°$ eastwards compared to to Ctrl simulation. The meridional wind profile (Fig. 7f) is

similar to NCEP and Ctrl. The zonal wind in Fig. 7e indicates that the eastward shift in the jet is not particularly dramatic as in Ctrlτ_{d12}. In contrast, the CtrlZMτ_{d3} simulation has a zonal wind structure similar to Ctrlτ_{d12} simulation. This can be seen by comparing Fig. 7a, g. As before, the meridional wind profile (Fig. 7h) is also quite similar. In other words, even with the differences in magnitude and location of zonal wind, the vertical structure of the TEJ is similar in simulations and reanalysis.

5 Dependence of location and strength of the TEJ on the spatial distribution of heating

The significant shifts of the simulated TEJ in the different simulations and reanalysis, regardless of the presence of orography indicate that it is the location and distribution of latent heating rather than just sensible heating from the Tibetan Plateau that plays a major role in the existence and location of TEJ. During the monsoon season, the major source of heating in the tropics is latent heating and hence it is necessary to look at the role of latent heating. Although CAM-3.1 does show reasonable fidelity in determining the spatial features of the TEJ, the discrepancies in location and magnitude of the maximum velocity of the TEJ need to be understood.

The reasons for this behavior is explored by analyzing the spatial distribution of simulated and observed rainfall. As in Kucharski et al. (2009) and Davis et al. (2012), precipitation is used as a proxy for latent heating. This is because precipitation on the ground over a spatially significant region is almost entirely the net latent heat release in the air mass over that region. Since the TEJ is close to

the tropopause level, it can be expected that net latent heat release is reasonably correlated with precipitation. For further confirmation, the spatial correlation between the maximum latent heat release and surface precipitation at each grid point in the regions under consideration (described below) were computed. The correlations were found to be between 0.87 and 0.94.

To get a more quantitative estimate of the change in the precipitation pattern, centroid of the precipitation (P_c) was computed using the following equation:

$$x_c = \frac{\sum_i P_i x_i}{\sum_i P_i}, \quad y_c = \frac{\sum_i P_i y_i}{\sum_i P_i} \tag{1}$$

where,

x_c and y_c	are the zonal and meridional coordinates of the P_c,
P_i	is the precipitation at each grid point,
x_i and y_i	are the zonal and meridional distances from a fixed coordinate system, in each case the grid point where peak precipitation occurs.

The region chosen for calculating the average precipitation and centroid was 40°E–130°E, 16°S–36°N.

5.1 Differences in the spatial distribution of precipitation in reanalysis and Ctrl simulation

Figure 8a–d show the July precipitation of reanalysis and Ctrl. The contrast between reanalysis and Ctrl simulation is quite striking. Most noticeable discrepancies in Ctrl are (1) significantly reduced precipitation in northern Bay of Bengal, East Asia, western Pacific warm pool, (2) a
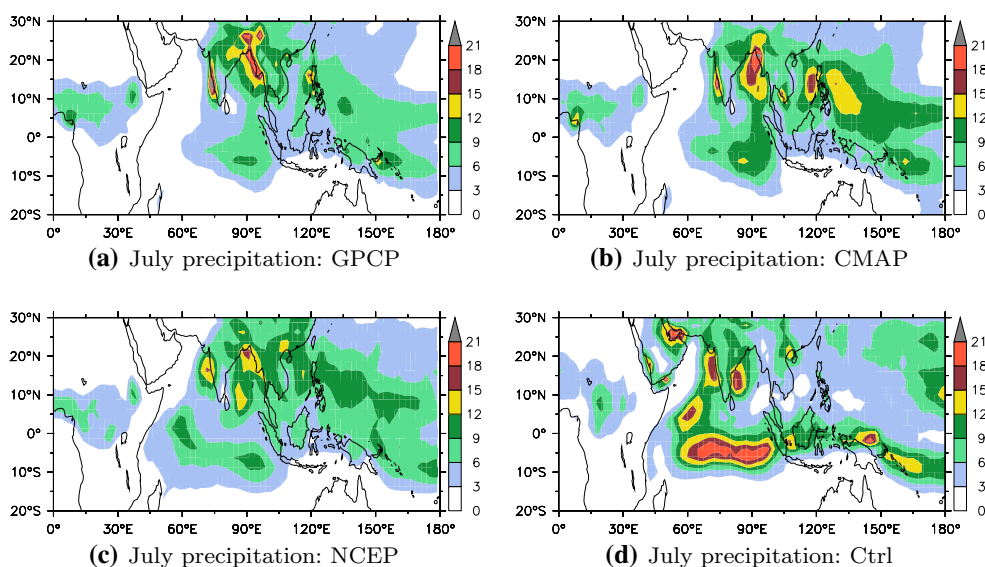

Fig. 8 Mean July precipitation (mm day^{-1}) of reanalysis and Ctrl simulation (color figure online)

Fig. 9 a–c Mean July precipitation difference, *warm colors* indicate regions where Ctrl has excess precipitation and *cool colors* indicate regions where there is excess precipitation in reanalysis data; **d** NCEP precipitation difference (mm day^{-1}), *warm colors* indicate regions where excess precipitation occurred in July 1988 and *cool colors* indicate regions where excess precipitation occurred in July 2002 (color figure online)

(a) July precipitation difference (Ctrl–GPCP)

(b) July precipitation difference (Ctrl–CMAP)

(c) July precipitation difference : Ctrl - NCEP

(d) Precipitation difference : NCEP (July 1988 – July 2002)
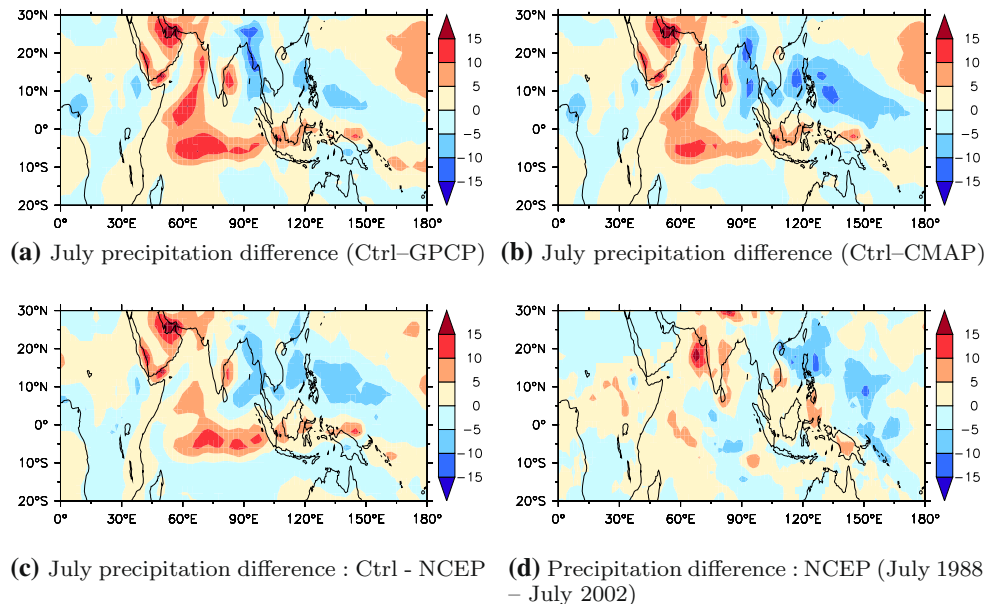
significant precipitation tongue just south of the equator between 50°E–100°E, and (3) spurious precipitation in the Saudi Arabian region that is approximately equal in magnitude to the precipitation peaks in central Arabian Sea and south-western Bay of Bengal. These discrepancies imply a major realignment in the local heating pattern. This unrealistic precipitation has been discussed by Hurrell et al. (2006). The reason for the incorrect simulation of precipitation in CAM-3.1, at least in the region of interest, appears to be partly due to SST gradients. In the Ctrl simulation, it was observed that, given warm enough temperatures and high enough low-level wind speeds, precipitation tended to be near regions where SSTs changed rapidly. The same was also observed in some aquaplanet simulations conducted by us (not shown). The reason for this behavior has not been explored.

From Table 1, it is seen that the mean precipitation in reanalysis is less than Ctrl simulation by ∼ 20 %, and the magnitude of U_{max} is also less by ∼ 25 %. There is also a ∼ 15° westward shift in the precipitation centroid in Ctrl compared to reanalysis data, similarly reflected in the location of U_{max}. Figure 9 shows these shifts. Figure 9a–c shows the differences between precipitation for Ctrl and reanalysis. It appears that, in Ctrl simulation, the westward shift in the peak of the simulated precipitation is consistent with the TEJ being centered over East Africa.

5.2 noGlOrog simulation

Precipitation pattern of noGlOrog simulation was similar to Ctrl simulation (not shown), although there was a reduction in the Bay of Bengal region. Choosing the same region for

precipitation as in Ctrl, it can be observed that even in this case, the shift is ∼ 20° westward in comparison to reanalysis (Table 1). As in Ctrl simulation, this westward shift is also reflected in the location of U_{max}. Based on this analysis, latent heating rather than orography has been shown to directly affect the location of the TEJ.

5.3 Simulations with modified cumulus parameterization

The same situation is observed even in the cases where the cumulus parameterization is changed. Figure 10a, b show the precipitation patterns for Ctrlτ_{d12} and noGlOrogτ_{d12} simulations. The eastward shift in the TEJ is consistent with the eastward shift in the precipitation. The TEJ is now in the correct location and matches closely with NCEP (Fig. 3a). From the first and third sections of Table 1, it is seen that the locations of U_{max} and precipitation centroid are in good agreement. Thus, it can be inferred that if the spatial pattern of rainfall is correctly captured, the TEJ will be correctly located. For the month of July, the spatial correlations between reanalysis and simulated precipitation in the region 40°E–130°E, 16°S–36°N were calculated. The correlations for Ctrl- and Ctrlτ_{d12}-reanalysis were 0.33 and 0.63 while that of CtrlZM-reanalysis and CtrlZMτ_{d3}-reanalysis were 0.49 and 0.68. This shows that when precipitation correlations are better, the spatial location of the TEJ is close to reanalysis. This again shows the importance of latent heating on the location of the TEJ.

The reduction in the magnitude of zonal winds speeds in noGlOrogτ_{d12} simulation may be related to the reduction in precipitation in the higher tropical latitudes in comparison
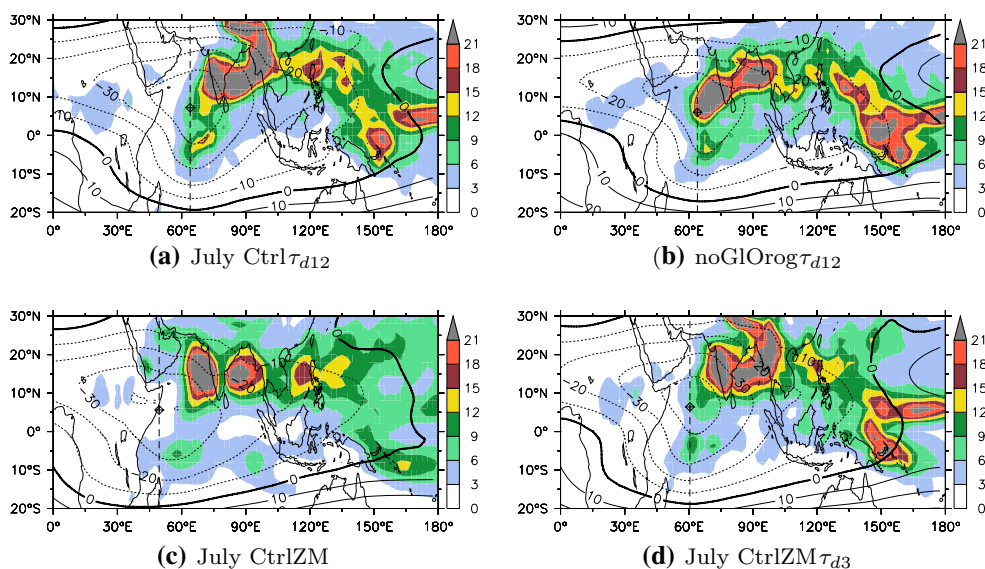
Fig. 10 July precipitation (mm day^{-1}, *shaded*) and zonal wind contours of CAM-3.1 simulations with modified Zhang–MacFarlane scheme. **a**, **b** Default Zhang–MacFarlane scheme with τ_d = 12 h; **c**, **d** Zhang–MacFarlane scheme from CESM-1.0.2 with τ_d = 1 and 3 h, respectively. Cross-sections are at pressure level where U_{max} is attained (refer Table 1), *cross-diamond* shows the location of maximum zonal wind. Data from simulations have been averaged for the month of July of five consecutive years (color figure online)

to Ctrlτ_{d12} (see Sect. 6 on aqua-planet simulations). The meridional wind profile of Ctrlτ_{d12} simulation also has the same shape as NCEP and Ctrl which again shows that the shift in the precipitation pattern has only altered the location of the TEJ. Although the overall precipitation is more in Ctrlτ_{d12} compared to Ctrl simulation by $\sim$ 25 % (see Table 1), there is a close match in the location of U_{max} in Ctrlτ_{d12} and noGlOrogτ_{d12}. In other words, the locations of the precipitation centroid and the TEJ are mutually consistent. The most significant change in rainfall pattern is, however, the total absence of precipitation in the Saudi Arabian region.

Similarly, the simulations with deep convective scheme of CESM-1.0.2 (Fig. 10c, d) also show the same features. There is a major improvement in some aspects. Precipitation in the Saudi Arabian region has reduced in comparison to Ctrl (Fig. 8d). The anomalous precipitation tongue just south of the equator has also reduced significantly, while that in the Pacific warm pool is more realistic as in Fig. 8a–c. This eastward shift in precipitation in CtrlZM simulation also hints at the fact that a reduction in heating in Saudi Arabian region may have caused the $\sim 7°$ eastwards shift of the TEJ in comparison to Ctrl. The magnitude and centroid of precipitation were calculated as before from Eq. (1). The meridional wind profile is similar. In case of CtrlZMτ_{d3} the precipitation is similar to Ctrlτ_{d12} simulation, with the added benefit that the overall magnitude of precipitation also reduced in comparison. As can be observed from Fig. 10a, d, there are relatively minor changes in the zonal wind structure and precipitation

pattern between these two simulations. These patterns are similar to Ctrl and NCEP (Table 1). Thus, it can be concluded that the spatial distribution of latent heating as well as its magnitude is an important factor influencing the location and structure of the TEJ. Only altering the portion of the model which changes the convective forcing determines the shape and location of the TEJ. Orography did not significantly influence the location of the jet. This does not imply that orography has no role in actively shaping the actual observed Asian monsoon. However, the location of the TEJ is correlated to the spatial distribution of monsoonal heat sources. If the simulated heat sources have a significantly different spatial distribution in comparison to reanalysis, then the simulated TEJ will also differ from the jet in reanalysis. This can be seen by comparing the with- and without-orography simulations. Also, as explained by Webster and Fasullo (2003), the presence of the TEJ results in convection; thus continues to fuel the jet in a feedback cycle. Although this feedback exists, it only enhances the coupling between the TEJ and the latent heating. It does not affect the general result that there is a significant relationship between the spatial distribution of precipitation and the location of the TEJ.

The shifts in the geopotential contours discussed before can now be understood in terms of the location of precipitation shifts. Since geopotential height at any level is related to the temperatures integrated form the surface to that layer, in the tropics the main mechanism that controls this is latent heat. The zonal wind at that layer is then related to the meridional gradient of geopotential height.

These conclusions are not limited to CAM-3.1 alone. The model used by Chakraborty (2004) also showed similar behavior (the GCM used was the same as that by Chakraborty et al. (2002, 2008). In this case also the TEJ was similar in simulations with and without orography (not shown). This happened because the precipitation patterns were similar in both simulations.

5.4 TEJ variability in reanalysis

As discussed in Sect. 3 and shown Fig. 4a, the location and strength of the TEJ in July 1988 and 2002 are quite different. The explanations above should be valid for reanalysis data as well. It is well known that in India 2002 was a drought year (Sikka 2003; Bhat 2006) while 1988 was an excess monsoon year (Ramesh et al. 1996). The relationship between precipitation and the jet location in the month of July for these 2 years is now clarified. Here, both precipitation and zonal winds from NCEP data because reanalysis winds are a product of forcing from the same data. If the TEJ is influenced largely by latent heating due to Indian summer monsoon then the July 2002 shift should be consistent with rainfall being shifted eastwards. This is seen in Fig. 9d, where the precipitation differences between July 1988 and 2002 are shown. There is a clear eastward shift in the rainfall distribution for July 2002, with the maximum being in the Pacific warm pool and relatively little in the Indian region. This is in contrast with July 1988, where Indian region receives high amounts of precipitation. The jet in 1988 peaks at 60°E–65°E while in 2002 the maximum is in the southern Indian peninsula implying a ∼20° westward shift. The same behavior for these 2 years was also observed in ERA40 data (not shown).

According to Rao et al. (2004), the strength of the TEJ has decreased between the years 1958 and 1998. This was correlated with a reduction in tropical cyclonic systems and summertime monsoonal depressions in the Bay of Bengal. This also agrees well with our results that reduced monsoonal heating leads to a reduction in the strength of the TEJ.

A reduction in the spatial extent of the TEJ between 1960 and 1990 was observed by Sathiyamoorthy (2005). According to the author, the near-disappearance of the jet over the Atlantic and African regions was related to the 4–5 decade prolonged drought conditions over the Sahel region.

This explanation is consistent with the results presented in this paper. Reduced latent heating in the Sahel region would lead to the TEJ being weaker, implying a weaker and smaller jet in this region.

6 Aqua-planet simulations

The appearance of the TEJ only during the months of Asian and Indian summer monsoon leads us to the question regarding the impact of spatial location of precipitation. Although rainfall is observed in the equatorial Inter-Tropical Convergence Zone (ITCZ) year round, no strong jet is observed year around. The zonal winds become strongest when there is a strong Continental Tropical Convergence Zone (CTCZ) with heavy precipitation located in the Bay of Bengal in JJA. To explore this issue, a series of aqua-planet simulations were conducted with single heat sources at 90°E, 10°N (AP_90e10n) and 90°E, 20°N (AP_90e20n), as discussed in Sect. 2.2. Precipitation was averaged in the region where SSTs were elevated. The region chosen for averaging was 70°E–110°E and 0°N–30°N.

In Table 2, the zonal winds and precipitation for these two simulations are shown. The zonal wind speed is about twice as high for the AP_90e20n simulation although the mean precipitation value is half that of the AP_90e10n simulation. This suggests that in the tropics, heating further away from the equator has more discernible impact on the zonal wind speed.

This is not a one-off phenomenon as many other similar simulations with different SST maxima have also been conducted (not shown). The maxima ranged from 23 to 37 °C. As before, all experiments had SSTs kept constant during the integration period. As the SST maxima were increased, so did the precipitation. The increase in precipitation was similar for heat sources centered at 10°N and 20°N, that is, for the same SST peak, both the heat sources induced similar amounts of mean precipitation. Whenever the heat source was centered at 90°E, 10°N the zonal wind speeds ranged from approximately 15 to 25 m s^{-1}. On the other hand, whenever the heat source was centered at 90°E, 20°N the zonal wind speeds ranged from approximately 15 to 55 m s^{-1}. This increase in zonal wind speed was monotonically increasing with mean precipitation for the 20°N heat source, but the 10°N heat source showed no such

Table 2 Magnitude (m s^{-1}) and location of peak zonal wind, and mean (mm day^{-1}) and centroid of precipitation in aqua-planet simulations

Case	Zonal wind				Precipitation		
	Peak	Lon (°E)	Lat (°N)	Press	Mean	Lon (°E)	Lat (°N)
AP_90e10n	21.76	82.5	10.0	175	8.93	90.1	14.5
AP_90e20n	42.20	82.5	10.0	150	4.88	90.7	19.4

pattern. Simulations with oval-shaped regions also gave the same results.

These simulations may partly explain the high jet strength only during the Indian summer monsoon season, because, during this period the northern Bay of Bengal receives significant amounts of rainfall. This is consistent with the model proposed by Gill (1980).

The increased jet zonal wind speeds in Ctrlτ_{d12} relative to noGlOrogτ_{d12} can be partly understood. In the former there was considerable precipitation to the north of 20°N. This may have contributed to the higher U_{max} values. However, the location of U_{max} has remained almost the same. This shows that the rainfall in the Assam hills may impact the jet strength and not its location.

7 Conclusions

The July climatological structure of the TEJ in observations has been compared with the simulations by an AGCM. The location of TEJ in reanalysis in July 1988 and 2002 had significant zonal shifts. Reduced precipitation in the Indian region in 2002 made the jet have its maxima in the southern Indian peninsula as compared to 1988, when high rainfall in the Indian region resulted in the TEJ having its maxima over the Arabian Sea region. This shows that the location of the TEJ is not completely influenced by orography.

The Ctrl simulation displayed errors in the location of the TEJ. When orography is removed, the spatial location and structure is relatively unchanged. This leads to the conclusion that the location of the TEJ is not directly influenced by orography, while the strength is affected due to slight changes in the spatial location and magnitude of precipitation. The primary reason for the shift in the simulated TEJ is that location of the precipitation in both Ctrl and noGlOrog is westwards when compared to reanalysis data.

Additional experiments were conducted to check if the TEJ is primarily influenced by latent heating. The aquaplanet simulations showed that heating in the higher tropical latitudes is more effective in generating jet velocities comparable to that of the TEJ. This offers an explanation about the reason for the jet to be very strong during the JJA monsoon season.

Changing the deep-convective relaxation time scale both in Ctrl and noGlOrog simulations confirmed this. In these new simulations, the precipitation is more accurately simulated and most importantly anomalous precipitation in Saudi Arabia no longer occurred. The jet followed the shift in precipitation and relocated to the correct climatological position. The absence of orography once again had no impact on the location of the jet. This provides significant evidence that the location of the TEJ is primarily dependent on the spatial distribution of precipitation. Replacing the default deep-convective cumulus scheme with that of CESM-1.0.2 also has the same effect on the jet. Both Ctrlτ_{d12} and CtrlZMτ_{d3} have very similar precipitation patterns and hence the location of the TEJ in both is correctly simulated.

References

Abish B, Joseph PV, Johannessen OM (2013) Weakening trend of the tropical easterly jetstream of the boreal summer monsoon season 1950–2009. J Clim 26:9408–9414. doi:10.1175/JCLI-D-13-00440.1

Adler RF, Huffman GJ, Chang A, Ferraro R, Xie PP, Janowiak J, Rudolf B, Schneider U, Curtis S, Bolvin D, Gruber A, Susskind J, Arkin P, Nelkin E (2003) The version-2 Global Precipitation Climatology Project (GPCP) monthly precipitation analysis (1979–present). J Hydrometeorol 4:1147–1167

Besson L, Lemaître Y (2014) Mesoscale convective systems in relation to African and tropical easterly tets. Mon Weather Rev 142:3224–3242

Bhat GS (2006) The Indian drought of 2002—a sub-seasonal phenomenon? Q J R Meteorol Soc 132(621):2583–2602. doi:10.1256/qj.05.13

Boos WR, Kuang Z (2010) Dominant control of the South Asian monsoon by orographic insulation versus plateau heating. Nature 463:218–222. doi:10.1038/nature08707

Bretherton CS, Peters ME, Back LE (2004) Relationships between water vapor path and precipitation over the tropical oceans. J Clim 17:1517–1528

Briegleb BP (1992) Delta-Eddington approximation for solar radiation in the NCAR Community Climate Model. J Geophys Res 97(D7):7603–7612. doi:10.1029/92JD00291

Camberlin P (1995) June-september rainfall in north-eastern Africa and atmospheric signals over the tropics. Int J Climatol 15(7):773–783. doi:10.1002/joc.3370150705

Chakraborty A (2004) Impact of orography on the simulation of monsoon climate in a general circulation model. PhD thesis, Indian Institute of Science, Bangalore

Chakraborty A, Nanjundiah RS, Srinivasan J (2002) Role of Asian and African orography in Indian summer monsoon. Geophys Res Lett 29(20):50-1–50-4. doi:10.1029/2002GL015522

Chakraborty A, Nanjundiah RS, Srinivasan J (2008) Impact of African orography and the Indian summer monsoon on the low-level Somali jet. Int J Climatol 29(7):983–992

Chen TC, van Loon H (1987) Interannual variation of the tropical easterly jet. Mon Weather Rev 115:1739–1759. doi:10.1175/1520-0493(1987)115<1739:IVOTTE>2.0.CO;2

Davis RN, Chen YW, Miyahara S, Mitchell NJ (2012) The climatology, propagation and excitation of ultra-fast Kelvin waves as observed by meteor radar, Aura MLS, TRMM and in the Kyushu-GCM. Atmos Chem Phys 12:1865–1879. doi:10.5194/acp-12-1865-2012

Duan AM, Wu GX (2005) Role of the Tibetan Plateau thermal forcing in the summer climate patterns over subtropical Asia. Clim Dyn 24:793–807. doi:10.1007/s00382-004-0488-8

Flohn H (1965) Thermal effects of the Tibetan Plateau during the Asian monsoon season. Correspondence, University of Bonn

Flohn H (1968) Contributions to a meteorology of the Tibetan highland. Atmospheric science paper 130. Colorado State University, Fort Collins

Gill AE (1980) Some simple solutions for heat-induced tropical circulation. Q J R Meteorol Soc 106(449):447–462

Gregory D, Kershaw R, Inness PM (1997) Parametrization of momentum transport by convection. II: Tests in single-column and general circulation models. Q J R Meteorol Soc 123:1153–1183

Hack JJ (1994) Parameterization of moist convection in the National Center for Atmospheric Research Community Climate Model (CCM2). J Geophys Res 99(D3):5551–5568. doi:10.1029/93JD03478

Hoskins BJ, Rodwell MJ (1995) A model of the Asian summer monsoon. Part 1: The global scale. J Atmos Sci 52:1329–1340. doi:10.1175/1520-0469(1995)052<1329:AMOTAS>2.0.CO;2

Hulme M, Tosdevin N (1989) The tropical easterly jet and Sudan rainfall: a review. Theor Appl Climatol 39(4):179–187. doi:10.1007/BF00867945

Hurrell JW, Hack JJ, Phillips AS, Caron J, Yin J (2006) The dynamical simulation of the Community Atmosphere Model version 3 (CAM3). J Clim 19:2162–2183. doi:10.1175/JCLI3762.1

Jain DK, Chakraborty A, Nanjundiah RS (2011) On the role of cloud adjustment time scale in simulating precipitation with relaxed Arakawa–Schubert convection scheme. Meteorol Atmos Phys 115:1–123. doi:10.1007/s00703-011-0170-8

Jingxi L, Yihui D (1989) Climatic study on the summer tropical easterly jet at 200 hPa. Adv Atmos Sci 6(2):215–226. doi:10.1007/BF02658017

Joseph PV (2012) Onset, advance and withdrawal of monsoon. In: Tyagi A, Asnani GC, De US, Hatwar HR, Mazumdar AB (eds) Monsoon monograph, vol 1. India Meteorological Department. http://www.imd.gov.in/section/nhac/dynamic/MM1.pdf

Kalnay E, Kanamitsu M, Kistler R, Collins W, Deaven D, Gandin L, Iredell M, Saha S, White G, Woollen J, Zhu Y, Chelliah M, Ebisuzaki W, Higgins W, Janowiak J, Mo KC, Ropelewski C, Wang J, Leetmaa A, Reynolds R, Jenne R, Joseph D (1996) The NCEP/NCAR 40-year reanalysis project. Bull Am Meteorol Soc 77:437–471. doi:10.1175/1520-0477(1996)077<0437:TNYRP>2.0.CO;2

Koteswaram P (1958) The easterly jet stream in the tropics. Tellus 10(1):43–57. doi:10.1111/j.2153-3490.1958.tb01984.x

Krishnamurti TN (1971) Observational study of the tropical upper tropospheric motion field during the northern hemisphere summer. J Appl Meteorol 10:1066–1096

Kucharski F, Bracco A, Yoo JH, Tompkins AM, Feudale L, Rutic P, Aquila D (2009) A Gill-Matsuno-type mechanism explains the tropical Atlantic influence on African and Indian monsoon rainfall. Q J R Meteorol Soc 135(640):569–579. doi:10.1002/qj.406

Lafore JP, Moncrieff MW (1989) A numerical investigation of the organization and interaction of the convective and stratiform regions of tropical squall lines. J Atmos Sci 46:521–544

Liu X, Yin ZY (2002) Sensitivity of East Asian monsoon climate to the uplift of the Tibetan Plateau. Palaeogeogr Palaeoclimatol Palaeoecol 183:223–245

Liu Y, Hoskins BJ, Blackburn M (2007) Impact of Tibetan orography and heating on the summer flow over Asia. J Meteorolog Soc Japan 85B:1–19. doi:10.2151/jmsj.85B.1

Mishra S (2010) Sensitivity of the simulated precipitation to changes in convective relaxation time scale. Ann Geophys 28:1827–1846. doi:10.5194/angeo-28-1827-2010

Mishra SK (2008) The impact of changes in temporal resolution and convective parameterization on the simulation of tropical climate in NCAR CAM3 GCM. PhD thesis, Indian Institute of Science, Bangalore

Nicholson SE, Barcilon AI, Challa M, Baum J (2007) Wave activity on the tropical easterly jet. J Atmos Sci 64:2756–2763. doi:10.1175/JAS3946.1

Raghavan K (1973) Tibetan anticyclone and tropical easterly jet. Pure Appl Geophys 110(1):2130–2142. doi:10.1007/BF00876576

Ramanathan V, Downey P (1986) A nonisothermal emissivity and absorptivity formulation for water vapor. J Geophys Res 91:8649–8666. doi:10.1029/JD091iD08p08649

Ramesh KJ, Mohanty UC, Rao PLS (1996) A study on the distinct features of the Asian summer monsoon during the years of extreme monsoon activity over India. Meteorol Atmos Phys 59:173–183

Rao BRS, Rao DVB, Rao VB (2004) Decreasing trend in the strength of tropical easterly jet during the Asian summer monsoon season and the number of tropical cyclonic systems over Bay of Bengal. Geophys Res Lett 31

Rasch PJ, Kristjánsson JE (1998) A comparison of the CCM3 model climate using diagnosed and predicted condensate parameterizations. J Clim 11:1587–1614. doi:10.1175/1520-0442(1998)011<1587:ACOTCM>2.0.CO;2

Raymond DJ, Blyth AM (1986) A stochastic mixing model for non-precipitating cumulus clouds. J Atmos Sci 43:2708–2718

Raymond DJ, Blyth AM (1992) Extension of the stochastic mixing model to cumulonimbus clouds. J Atmos Sci 49:1968–1983

Rayner NA, Parker DE, Horton EB, Folland CK, Alexander LV, Rowell DP (2003) Global analyses of sea surface temperature, sea ice and night marine air temperature since the late nineteenth century. J Geophys Res 108(D14):4407. doi:10.1029/2002JD002670

Reynolds RW, Rayner NA, Smith TM, Stokes DC, Wang W (2002) An improved in situ and satellite SST analysis for climate. J Clim 15:1609–1625. doi:10.1175/1520-0442(2002)015<1609:AIISAS>2.0.CO;2

Richter JH, Rasch PJ (2008) Effects of convective momentum transport on the atmospheric circulation in the community atmosphere model, version 3. J Clim 21:1487–1499

Sathiyamoorthy V (2005) Large scale reduction in the size of the tropical easterly jet. Geophys Res Lett 32(14):L14802. doi:10.1029/2005GL022956

Sikka DR (2003) Evaluation of monitoring and forecasting of summer monsoon over India and a review of monsoon drought of 2002. Proc Indian Natl Sci Acad Part A 69(5):479–504

Slingo A (1989) A GCM parameterization for the shortwave radiative properties of clouds. J Atmos Sci 46:1419–1427. doi:10.1175/1520-0469(1989)046<1419:AGPFTS>2.0.CO;2

Uppala SM, Kallberg PW, Simmons AJ, Andrae U, Bechtold VD, Fiorino M, Gibson JK, Haseler J, Hernandez A, Kelly GA, Li X, Onogi K, Saarinen S, Sokka N, Allan RP, Andersson E, Arpe K, Balmaseda MA, Beljaars ACM, Berg LVD, Bidlot J, Bormann N, Caires S, Chevallier F, Dethof A, Dragosavac M, Fisher M, Fuentes M, Hagemann S, Holm E, Hoskins BJ, Isaksen L, Janssen PAEM, Jenne R, McNally AP, Mahfouf JF, Morcrette JJ, Rayner NA, Saunders RW, Simon P, Sterl A, Trenberth KE, Untch A, Vasiljevic D, Viterbo P, Woollen J (2005) The ERA-40 re-analysis. Q J R Meteorol Soc 131(612):2961–3012. doi:10.1256/qj.04.176

Wang B (2006) The Asian monsoon. Springer

Webster PJ, Fasullo J (2003) Monsoon: dynamical theory. In: Encyclopedia of atmospheric sciences. Academic Press, London, pp 1370–1385

Xie P, Arkin PA (1997) Global precipitation: a 17-year monthly analysis based on gauge observations, satellite estimates, and numerical

model outputs. Bull Am Meteorol Soc 78(11):2539–2558. doi:10.1175/1520-0477(1997)078<2539:GPAYMA>2.0.CO;2

Ye D (1981) Some characteristics of the summer circulation over the Qighai-Xizang (Tibet) Plateau and its neighborhood. Bull Am Meteorol Soc 62:14–19. doi:10.1175/1520-0477(1981)062<0014:SCOTSC>2.0.CO;2

Zhang GJ, McFarlane NA (1995) Sensitivity of climate simulations to the parameterization of cumulus convection in the Canadian Climate Centre general circulation model. Atmos Ocean 33(3):407–446. doi:10.1080/07055900.1995.9649539

Zhang M, Bretherton CS, Hack JJ, Rasch PJ (2003) A modified formulation of fractional stratiform condensation rate in the NCAR Community Atmospheric Model CAM2. J Geophys Res 108(D1):ACL 10-1–ACL 10-11. doi:10.1029/2002JD002523

Zhang Q, Wu G, Qian Y (2002) The bimodality of the 100 hPa South Asia high and its relationship to the climate anomaly over East Asia in summer. J Meteorol Soc Jpn 80(4):733–744. doi:10.2151/jmsj.80.733